Supporting Information

Chirality-Induced Second Harmonic Generation in Supramolecular 4-Nitro-D-Phenylalanine Hybrid Crystal

Ye Tan,[a] Qing-Ju Gao,[a] Wen-Shuang Mu,[a] Xing-Guo Xiang,[a] Gao-Yu Zhao,[a,*] Jingyu Guo,[c] Zhihua Yang,[d] Ling Chen[b,c*]

[a.]School of Chemical Engineering, Guizhou University of Engineering Science, Xueyuan Road, Qixingguan District, Bijie, 551700, People's Republic of China.

[b.]State Key Laboratory of New Textile Materials and Advanced Processing, Wuhan Textile University, Wuhan 430200, People's Republic of China

[c.]Center for Advanced Materials Research, Advanced Institute of Natural Sciences, Beijing Normal University, Zhuhai 519087, People's Republic of China.

[d.]Research Center for Crystal Materials, Xinjiang Technical Institute of Physics and Chemistry, Chinese Academy of Sciences, Urumqi, People's Republic of China.

EXPERIMENTAL METHODS

Materials. 4-nitro-D-phenylalanine and 4-nitro-L-phenylalanine were purchased from Innochem Technology Co., Ltd.

4-nitro-D-phenylalanine nitrate [D-NPA**]**

4-nitro-D-phenylalanine (5 mmol, 1.050 g) and 10 mL H_2O were taken in a beaker (50 mL), 1.00 mL HNO_3 was added dropwise to the suspension, then heated it to 80 ℃ until the solution was completely clear and slowly cooled it to room temperature. After standing for 14 days, light yellow rod-shaped crystals were obtained with a yield of 78%. Large crystal of D-NPA is obtained by suspending the seed crystal in its saturated solution (Size of large crystal: 31 × 5 × 4 mm, see the inset of Fig. 2c).

Rac-NPA was synthesized by replacing 5 mmol 4-nitro-D-phenylalanine with 2.5 mmol 4-nitro-D-phenylalanine and 2.5 mmol 4-nitro-L-phenylalanine using the same method. After standing for 20 days, light yellow needle-like crystals were obtained (inset of Fig. 2d).

Characterization

X-ray diffraction data were collected using a Bruker D8 QUEST/VENTURE single-crystal diffractometer. The crystallographic data and refinements are presented in Tables S1. UV−vis diffuse reflectance spectra were determined at room temperature on a Shimadzu UV-3600i Plus spectrophotometer. Infrared spectra were acquired on a ThermoFisher Nicolet Is5 FTIR spectrometer. Thermogravimetry (TG) and differential scanning calorimetry (DSC) analyses were performed with a METTLER TOLEDO TGA/DSC 3+ thermal analyzer instrument under N_2 atmosphere. The SHG efficiency was measured via the Kurtz powder method with the assistance of a Mini-NOTS 1064 SHG NLO testing instrument. The electronic structure and optical properties were calculated using the Vienna Ab initio Simulation Package (VASP) based on the principles of Density Functional Theory (DFT).

Circular dichroism (CD) measurement:

Linear circular dichroism (CD) spectra were obtained using a JASCO J-810 CD

spectrometer. The specific procedure is as follows: the sample was thoroughly mixed with dry potassium bromide (KBr) powder at a mass ratio of 0.5% (sample/KBr). The mixture was then finely and uniformly ground and pressed at approximately 7 tons using a hydraulic press to form a transparent pellet. The pellet was subsequently placed in the sample holder of a CD spectrometer, and the CD spectrum was recorded over the wavelength range of 200-600 nm.

Computational Methods

The electronic and band structures as well as linear optical property calculations were performed by employing CASTEP[1]. Generalized gradient approximation (GGA)[2] as parametrized by Perdew-Burke-Ernzerhof (PBE) is used to calculate optical properties.[3] H1s^1, C 2$s^2$2p^2, N 2$s^2$2p^3 and O 2$s^2$2p^4 electrons are treated as valence electrons, and all the other electrons are treated as core electrons. The plane-wave energy cutoff was set at 900.0 eV, and the k-point separation for each material was set as 0.04 $Å^{-1}$ in the Brillouin zone. In order to ensure the convergence of the optical properties, the empty bands are set to three times the valence bands in the calculation. The hybrid HSE06[4] generalized function implemented in the PWmat[5] code was used to calculate the bandgap values more accurately with the NCP-SG15-PBE pseudopotential. The bandgap difference between GGA and HSE06 is used as a scissor operator to calculate the birefringence and SHG coefficients.

Table S1. Crystallographic parameters of D-NPA and rac-D-NPA

Compound	D-NPA	rac-D-NPA
CCDC number	2415224	2439970
Molecular formula	$C_9H_{11}N_3O_7$	$C_9H_{11}N_3O_7$
Formula weight	273.21	273.21
Crystal color	Light yellow	Light yellow
Crystal system	orthorhombic	monoclinic
Space group	$P2_12_12_1$	$P2_1/c$
a (Å)	5.672(4)	13.9826(6)
b (Å)	7.971(6)	5.6016(3)
c (Å)	26.69(2)	15.9230(8)
β (°)	90	104.970(2)
V (Å^3)	1206.70(154)	1204.84(10)
Z	4	4
Dc.(g/cm^3)	1.504	1.506
Flack parameter	0(4)	/
μ (mm^{-1})	0.710	0.710
GOOF on F^2	1.018	1.041
R_1, wR_2 $I>2\sigma(I)$	0.0495, 0.1105	0.0384, 0.0945
R_1, wR_2 (all data)	0.0842, 0.1386	0.0488, 0.1018
Largest diff peak/hole, e·Å^{-3}	0.238/-0.202	0.584/-0.278

Table S2. Atomic coordinates of D-NPA

Atom	*Wyckoff*	*x*	*y*	*z*
O4	4a	0.5382(7)	0.7782(4)	0.47370(15)
O3	4a	0.3926(10)	0.9242(5)	0.41033(18)
N2	4a	0.2769(7)	0.5101(5)	0.45471(15)
H2A	4a	0.170581	0.431959	0.447158
H2B	4a	0.250648	0.547867	0.485594
H2C	4a	0.420804	0.465959	0.453048
O7	4a	0.5720(7)	1.1969(5)	0.44605(19)
O6	4a	0.7886(7)	1.4138(5)	0.44263(17)
N3	4a	0.7756(8)	1.2590(6)	0.44561(17)
O5	4a	0.948827	1.171299	0.450001
N1	4a	-0.271713	0.081491	0.287646
O1	4a	-0.426730	0.123977	0.258110
C8	4a	0.257919	0.650756	0.418663
C9	4a	0.413312	0.790543	0.437784
C1	4a	-0.112748	0.216415	0.305689
C4	4a	0.173577	0.464399	0.343331
C5	4a	-0.032026	0.505229	0.317339
H5	4a	-0.073088	0.617310	0.313159
O2	4a	-0.235379	-0.060825	0.301176
C3	4a	0.230701	0.297679	0.348666
H3A	4a	0.369881	0.268862	0.364954
C7	4a	0.328537	0.598795	0.365505
H7A	4a	0.323226	0.696820	0.344001
H7B	4a	0.489989	0.558697	0.366048
C6	4a	-0.174555	0.382256	0.297849
H6	4a	-0.309408	0.409771	0.279811
C2	4a	0.087106	0.172265	0.330509
H2	4a	0.126001	0.059986	0.335126
H3	4a	0.486837	1.016627	0.421624
H8	4a	0.079282	0.691116	0.417789

Table S3. Total energies calculated at the B3LYP/6-31G(d) level

Compound	E/a.u.	ΔE/kcal·mol^{-1}
rac-NPA	-1039.9517268	0.00
D-NPA	-1039.9357919	10.00

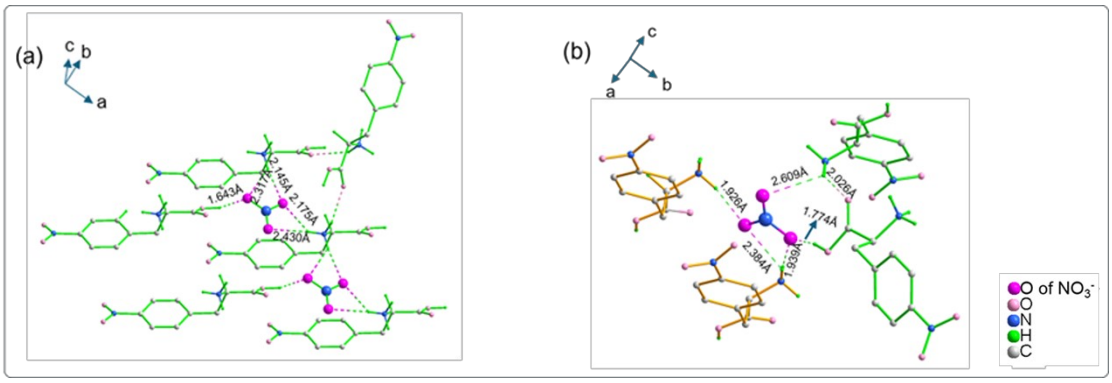

Figure S1. (a) Hydrogen bonds of D-NPA between protonated 4-nitro-D-phenylalanine cations and NO_3^- anions. (b) Hydrogen bonds of rac-NPA between protonated 4-nitro-D(L)-phenylalanine cations and NO_3^- anions.

Birefringence measurement:

Since the natural grown crystal surface of D-NPA doesn't always follow a specific optical principal axis, the measured refractive index differences are smaller than the actual birefringence. The crystal thickness of is 28.0 μm. And the optical path difference is 3.55 μm at 1064 nm. According to the following formula:

$$R = |Ng - Np| * d = \Delta n * d$$

where R represents the optical path difference; N_g and N_p are the refractive indices of the fast light and slow light, respectively; Δn is the difference value in refractive index values; and d denotes the thickness of the crystal. Therefore, the refractive index difference is 0.131 at 1064 nm.

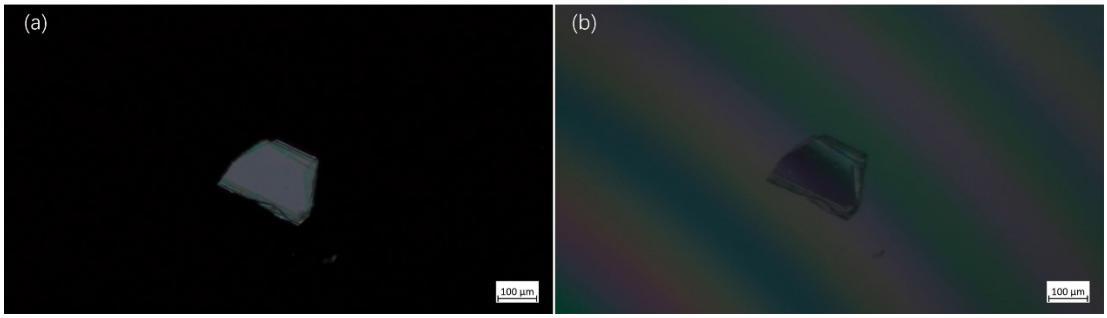

Figure S2. The birefringence measurement of D-NPA.

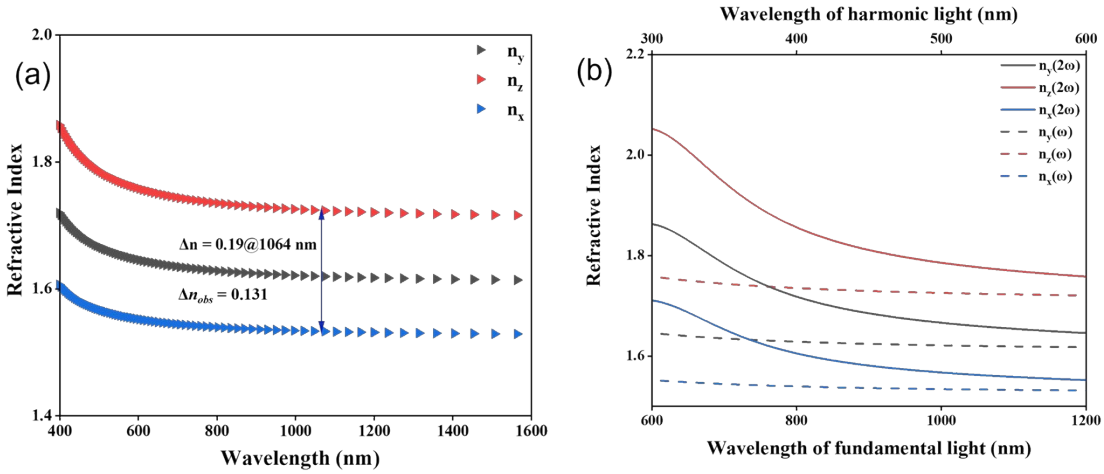

Figure S3. (a) Refractive index dispersion curves of D-NPA. (b) Theoretical refractive dispersion curves for the fundamental light (dashed line) and the frequency-doubled one (solid line) of D-NPA.

Table S4. Real-space atom-cutting (RSAC) analysis of fragment contributions in D-NPA.

structures	d_{14}
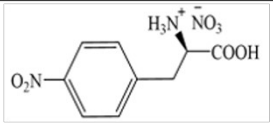	1.41
$C_9H_{11}N_3O_7$ [D-NPA]	
NO_3	-0.05
COOH	0.01
NH_3	0.00
C_2H_3	0.02
C_6H_4	0.36 (47%)
NO_2	0.43 (56%)
total	0.77

Table S5. RSAC-d_{14} analysis of D-NPA and its organic moiety.

structures	d_{14}
$C_9H_{11}N_3O_7$ [D-NPA]	1.41
$C_9H_{11}N_2O_4$	1.46(103%)

Table S6. CASTEP-based computational results for D-NPA.

Compound	GGA (eV)	HSE06(eV)	$\lvert d_{ij} \rvert$ (pm/V)	Δn (@1064 nm)	PM (nm)
D-NPA	2.49	3.88	d_{14} = 1.41	0.19	368

References

1. G. J. Ackland, Embrittlement and the bistable crystal structure of zirconium hydride, *Phys. Rev. Lett.*, 1998, **80**, 2233-2236.
2. J. P. Perdew, K. Burke and M. Ernzerhof, Generalized gradient approximation made simple, *Phys. Rev. Lett*., 1996, **77**, 3865-3868.
3. N. Govind, M. Petersen, G. Fitzgerald, D. King-Smith and J. Andzelm, A generalized synchronous transit method for transition state location, *Comp. Mater. Sci.*, 2003, **28**, 250-258.
4. J. Heyd and G. E. Scuseria, Efficient hybrid density functional calculations in solids: assessment of the Heyd-Scuseria-Ernzerhof screened Coulomb hybrid functional, *J. Chem. Phys.*, 2004, **121**, 1187-1192.
5. S. Wu, X. L. Yang, H. S. Zhang, L. Shi, Q. Zhang, Q. Y. Shang, Z. M. Qi, Y. Xu, J. Zhang, N. Tang, Y. T. Wang, W. K. Ge, B. Shen and X. Q. Pan, Unambiguous identification of carbon location on the N site in semi-insulating GaN, *Phys. Rev. Lett.*, 2018, **121**, 145505.